Enhanced superconductivity, Kondo behavior, and negative-curvature resistivity of oxygen-irradiated thin films of aluminium

E. H. C. P. Sinnecker, M. M. Sant'Anna, and M. ElMassalami*

Instituto de Física, Universidade Federal do Rio de Janeiro, Caixa Postal 68528, Rio de Janeiro, Rio de Janeiro 21941-972, Brazil

(Received 20 June 2016; revised manuscript received 27 January 2017; published 23 February 2017)

We followed the evolution of the normal and superconducting properties of Al thin films after each session of various successive oxygen irradiations at ambient temperature. Such irradiated films, similar to the granular ones, exhibit enhanced superconductivity, Kondo behavior, and negative-curvature resistivity. Two distinct roles of oxygen are identified: as a damage-causing projectile and as an implanted oxidizing agent. The former gives rise to the processes involved in the conventional recovery stages. The latter, considered within the context of the Cabrera-Mott model, gives rise to a multistep process which involves charges transfer and creation of stabilized vacancies and charged defects. Based on the outcome of this multistep process, we consider (i) the negative-curvature resistivity as a manifestation of a thermally assisted liberation of trapped electric charges, (ii) the Kondo contribution as a spin-flip scattering from paramagnetic, color-center-type defects, and (iii) the enhancement of T_c as being due to a lattice softening facilitated by the stabilized defects and vacancies. The similarity in the phase diagrams of granular and irradiated films as well as the aging effects are discussed along the same line of reasoning.

DOI: 10.1103/PhysRevB.95.054515

I. INTRODUCTION

Generally, controlled incorporation of a chemically active element into a metallic superconducting thin film induces a drastic modification in its normal and superconducting phase diagram [1,2]. The modification in the superconductivity can be illustrated by the increase of the transition points, T_c, of oxygen-incorporated Al films by up to a factor of three [3–6]. The modifications in the normal state, on the other hand, are not less spectacular: (i) Although both Al and O are nonmagnetic, oxygen-incorporated Al film exhibits a (∼10 K) Kondo behavior that competes with the superconducting state [3,4], and (ii) its resistivity exhibits a negative curvature (NCR) at ∼300 K with a deviation downwards away from the *linear-in-T* behavior [3,4].

It is remarkable that (i) these induced features are evident in both the granular films [1–4] (oxygen is incorporated during the codeposition process) and irradiated films [6] (oxygen is implanted posterior to film synthesis), (ii) the T_c enhancement follows a domelike behavior [3,4,7] reminiscent of the case of HTc cuprates, and (iii) the NCR feature is unique and has no resemblance to the recovery stages usually observed in *pure* Al films [8].

Historically, the induced features of granular films had been treated separately from those appearing in irradiated ones. Similarly, each feature had been treated as if independent of the others. Moreover, none of them had been correlated with the kinetics of defects (interstitials, vacancies, etc.; see Fig. 1) even when these are introduced by such a damage-causing irradiation process. As a result of these historical approaches, much of the essential features (and their driving mechanisms) of the normal and superconducting phase diagrams of the irradiated and granular films are not well clarified.

In this work we systematically studied the evolution of the normal and superconducting properties of Al thin film when oxygen is progressively incorporated via irradiation at ambient temperature. A phase diagram is constructed from the events manifested in the resistivity curves. We analyzed such a phase diagram and identified the region of operation for each of NCR, the Kondo behavior, and the enhancement of T_c. We discuss the mechanisms involved in each effect.

Our experimental methods and materials are presented in Sec. II, the results and analysis are in Sec. III, while the discussion and a summary are given in Sec. IV.

II. EXPERIMENTAL

Thin films of 400 μm × 10 μm × 90 nm were prepared at room temperature by sputtering Al on a lithographed Si/SiO_2 substrate with Ti/Au contact pads. Electron microscopy images indicate a grain size of ∼60 nm. Such thin films were irradiated [9] with O^- ions at room temperature; seven consecutive implantation sessions were carried out (see Table I). We observed no significant dependence of the studied properties on the implantation depth profile when using energies of 10, 23, or 30 keV.

The influence of each irradiation was followed by DC/AC four-point resistivity measurements both *in situ,* during irradiations, as well as *ex situ.* The latter ones were measured as a function of time, temperature, magnetic field, and fluence after each nth irradiation session: $\rho(t,T,H,n\text{th})$. Routinely, $\rho(T,H,n\text{th})$ was measured, directly after nth irradiation, during the cooling down to ∼1.7K and, afterwards, the warming up to ∼320 K: Except for aging effects, the measurements were reproducible and the obtained curves compare favorably with the ones reported for granular [1–4] and irradiated films [6]. Hall measurements on representative samples confirmed the earlier findings [10] that the major charge carriers are electrons and their density decreases with irradiation.

Based on analysis of thermal evolution of each $\rho(t,T,H,x)$ curve, we identified all transition and crossover events. A plot of these temperature points versus x gives the $T-x$ phase diagram of the O-irradiated thin films (x is the tunable parameter). We include in this very same phase diagram *all* the previously reported $T(x)$ of granular [1–4] and irradiated thin

*massalam@if.ufrj.br

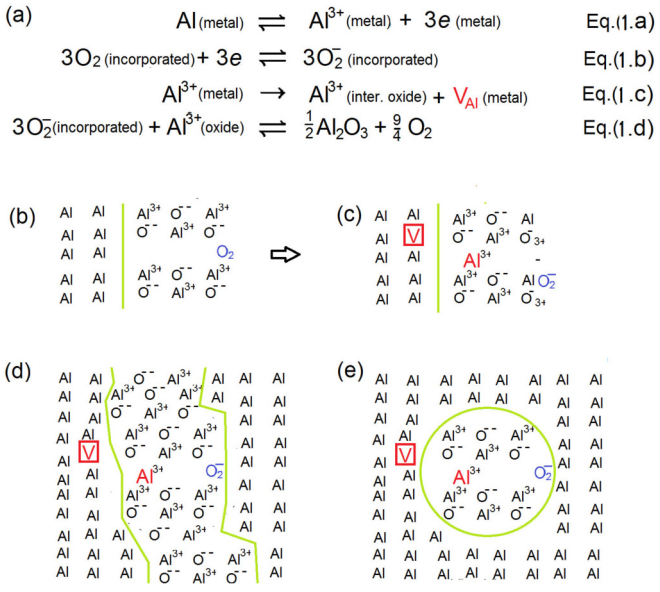

FIG. 1. (a) A multistep kinetic scheme for oxidation of aluminum as described in the Cabrera-Mott model (adapted from Ref. [12]). Directly after ionization [Eq. (1a)], electrons pass freely through the oxide interface until reaching incorporated oxygen which are then ionized to O_2^- [Eq. (1b)]. This charge transfer together with the left-behind positive Al^{3+} induce a local electric field which drives the slow migration of Al^{3+} across the oxide interface, leaving behind a vacancy V_{Al} [Eq. (1c)]. Equation (1d) indicates a typical formation of Al_2O_3 by the combination of migrated Al^{3+} and ionized O_2^-. Panels (b) and (c): Illustration of the reaction at metal-oxide interface (represented by the solid green line) of a directly exposed film [panel (b) is before an event of Eq. (1a) while panel (c) is after the event of Eq. (1c); adapted from Ref. [13]]. (d) We consider that, during the codeposition process of a granular film, the incorporated oxygen does not enter as an idle and neutral entity, rather it does react with Al matrix, just as in the normal oxidation process of Cabrera-Mott, leading to an interaction similar to that described in panels (a)–(c). Ultimately this accumulates into an extended nanosized grain. (e) Similar reaction occurring at the boundary of an isolated oxide grain of an irradiated film. In all cases, incorporated and ionized oxygen are represented, with no loss of generality, by O_2 and O_2^-.

films [6]. It is worth mentioning that many of the reported $T_c(x)$ values were given as a function of $\rho_{300\,\mathrm{K}}$ (see, e.g., Refs. [3,4]). Here, we maintain the same convention which, due to relaxation effects, corresponds to our extrapolated $\rho^{\mathrm{ext}}_{300\,\mathrm{K}}$: At any rate this is essentially a parameter which can be substituted, with no loss of generality, by x or ρ_o (the latter tracks the combined influence of the parameters appearing in $\rho_o = m/n\tau e^2$; all terms have their usual meanings).

III. RESULTS

A. The two classes of relaxation processes

Oxygen implantation is a violent process that leads to an unstable state. A drive towards equilibrium requires an activation of some relaxation channels. Different from neutron or electron irradiation [8], O irradiation provides additional process(es) related to the Cabrera-Mott oxidation process [15] (see Fig. 1). Therefore, one expects (see Fig. 2) two classes of relaxation processes. The first class consists of conventional, relatively fast, relaxation processes [8], which are manifested, for pure Al, as three recovery stages [8]: Stage I is dominant below ∼50 K; stage II is centered at ∼140 K, while stage III operates within $190 < T < 250$ K. The second class consists of much slower (in weeks) relaxation processes and are dominant at sufficient O-implantation level and higher temperatures, $T > 250$ K. As can be seen in Eqs. (1a)– (1d) of Fig. 1, the overall process involves charge transfer, charge trapping, vacancies creation, defect migrations and annihilation, etc. [13]. We show below that the processes associated with the second class are the driving factors behind the above-mentioned modifications in the phase diagram.

It is worth mentioning that (i) the reaction involving Eqs. (1a)– (1d) continues until equilibrium is established via opposing forces related to diffusion and disassociation. (ii) Oxidation in both the granular and irradiated films, in contrast to the exposed case, occurs within the film bulk/profile depth and, furthermore, the involved quantity of oxygen is fixed after ending the incorporation process. (iii) For the particular case of irradiated film, the initial uniformly distributed out-of-equibrium state relaxes back to equilibrium via the same two relaxation processes. As far as the incorporated oxygen is concerned, its reaction is similar to the oxidation process described by Eqs. (1a)– (1d). Ultimately, this leads to an incipient germination of centres of Al_2O_3 which with further kinetics accumulates into a nanosized bubble: The limitation

TABLE I. Beam energy, partial and accumulated fluence, and peak center of depth profile for each of the consecutive implantation sessions used in this work. The specific range of energies were chosen to probe any dependence on implantation profile: as that no significant dependence was observed, all subsequent implantations (4th to 7th) were performed with a beam of 23 keV.

Irradiation session	Energy (keV)	Peak of depth profile[a] (nm)	Fluence (10^{16} ions/cm^2)	Accumulated fluence (10^{16} ions/cm^2)
1	23	50	0.42	0.42
2	10	23	0.34	0.76
3	30	64	0.50	1.26
4	23	50	1.21	2.47
5	23	50	1.25	3.72
6	23	50	1.77	5.49
7	23	50	0.97	6.46

[a]Estimated using the SRIM code [11].

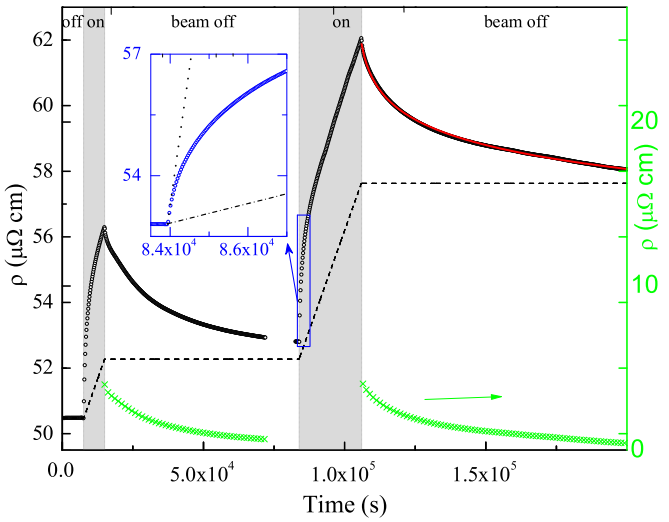

FIG. 2. $\rho(t,300\,\mathrm{K},6\mathrm{th})$ measured with a current density $j = 10^7\mathrm{A/m}^2$ during two consecutive O-irradiation sessions without breaking a vacuum of 1.0×10^{-7} Torr. The irradiation intervals are shown as vertical gray areas. The inset highlights the presence of relaxation processes: In their absence, the resistivity rise should have followed the dotted line. During the steady state, the resistivity rises linearly with a rate given by the dot-dashed line in the inset. Directly after beam stoppage, there are two contributions: a fast-decaying one governed by one class of relaxations (depicted as green crosses with values given by the right-hand y axis) and a slow contribution governed by a second class of relaxations; the latter is evident as a weak decay in the almost horizontal, dashed lines. The fast-decaying $\rho_d(t > 106000\,\mathrm{s}, 300\ \mathrm{K}, 6\mathrm{th})$ is well fitted to Eq. (5) of the first of Refs. [14] (solid red line).

into nanosize grains is identical to the case of nanosized Al_2O_3 surface in conventional oxidation of metallic Al.

B. The negative-curvature resistivity (NCR)

Resistivity curves $\rho(1.7 \leqslant T \leqslant 315\ \mathrm{K}, n\mathrm{th})$ of Fig. 3(a) indicate conclusively that the surge of $T_c(x)$ enhancement [Fig. 3(c)], the Kondo behavior [Figs. 3(e) and 4(b)], as well as the NCR effect [Fig. 4(a)] are correlated with each other and that all are much accentuated with each subsequent nth irradiation [Fig. 3(a)]. These features were not observed in conventional recovery stages; accordingly they must be associated with the second class of relaxation processes. In addition, there are aging effects that are much accentuated for $T > T_{\mathrm{NCR}}$; in contrast, there are no signs of aging in $\rho(t, T < T_{\mathrm{NCR}}, 7\mathrm{th})$ even when the film is repeatedly recycled within $T < T_{\mathrm{NCR}}$. The manifestation of a slow (in weeks) aging of both the position of T_{NCR} and the magnitude of $\rho(T_{\mathrm{NCR}})$ rules out any interpretation in terms of crystalline electric field splitting. It is worth adding that a similar aging effect had not been explicitly studied in Al granular film and that linear-in-T behavior for granular films were observed only for samples with $\rho_{300\,\mathrm{K}} < 100\,\mu\Omega\,\mathrm{cm}$.

After three months, $\rho(T, 7\mathrm{th})$ traverses the NCR peak reversibly and with no hysteresis (though with a lower magnitude and a higher T_{NCR}): This nonhysteresis feature can be identified in the reported results of granular Al films [3,4].

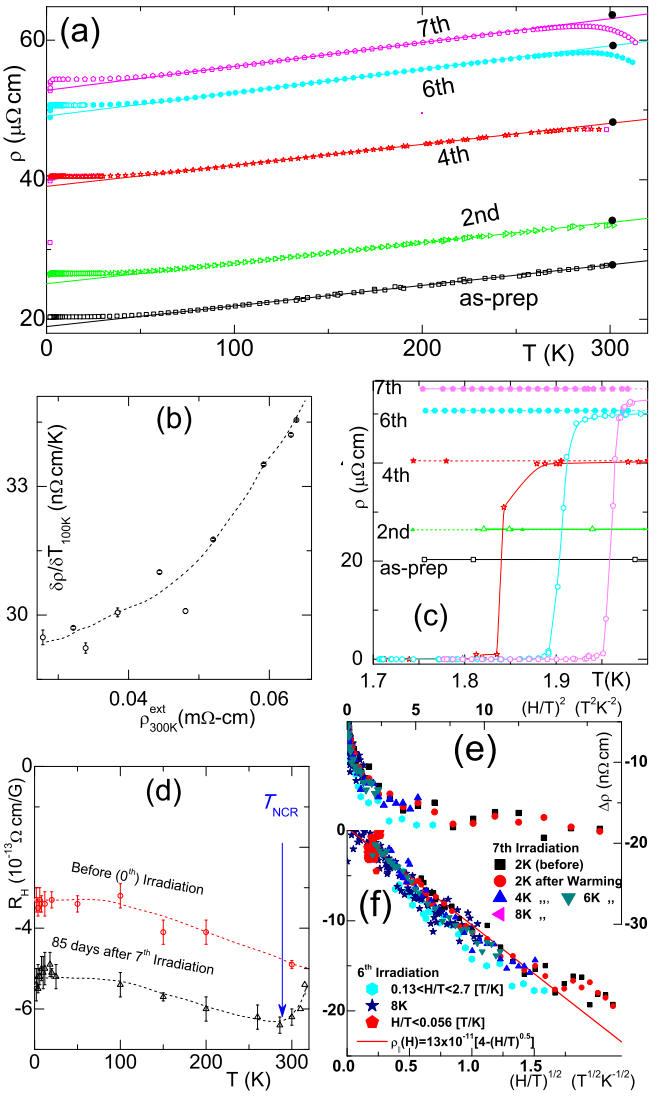

FIG. 3. (a) Representative $\rho(T,n\mathrm{th})$ curves. The solid lines are linear fit with a slope $(\partial\rho/\partial T)_{100\text{-}220\mathrm{K}}$. Due to aging effects, a unique room-temperature resistivity for each warming-up measuring cycle is taken to be the extrapolated $\rho^{\mathrm{ext}}_{300\,\mathrm{K}}$, solid circle on the high-T linear extrapolation. (b) Evolution of $(\partial\rho/\partial T)_{100\text{-}220\mathrm{K}}$ as a function of $\rho^{\mathrm{ext}}_{300\,\mathrm{K}}$. (c) An expanded view of low-T $\rho(T,H,n\mathrm{th})$ curves of panel a. Open (solid) symbols denote zero-field (5kOe) curve. (d) Hall coefficients of as-prepared film and that of the same film measured 85 days after the 7th irradiation. (e) $\Delta\rho(H/T, n\mathrm{th}) = \rho(H/T, n\mathrm{th}) - \rho(0, T, n\mathrm{th})$ versus $(H/T)^2$: showing the breakdown of the $(H/T)^2$ scaling. These curves are from $n\mathrm{th} = 6$, 7 irradiation and are limited to the range of $H_{c2} < H < 20$ kOe and $T_c < T < T_{\mathrm{K}}^{mn}$ (small H/T). (f) The same as panel e but are scaled to $\sqrt{H/T}$. This better scaling is emphasized by the solid line fit $\Delta\rho(H/T, 6\mathrm{th}) \propto (H/T)^{1/2}$.

The similarity in both the reported and our T_{NCR} (see plot of Fig. 5) reveals a similarity in the mechanism behind this NCR.

Figure 3(d) indicates that the conductivity enhancement $(T > T_{\mathrm{NCR}})$ occurs concomitantly with a decrease in the magnitude of Hall coefficient. We associate the NCR event to a thermally assisted liberation of trapped charges (with a binding potential of $\sim k_B T_{\mathrm{NCR}}$). Such trapped charges are possibly electrons (neighboring an anionic vacancy) or holes

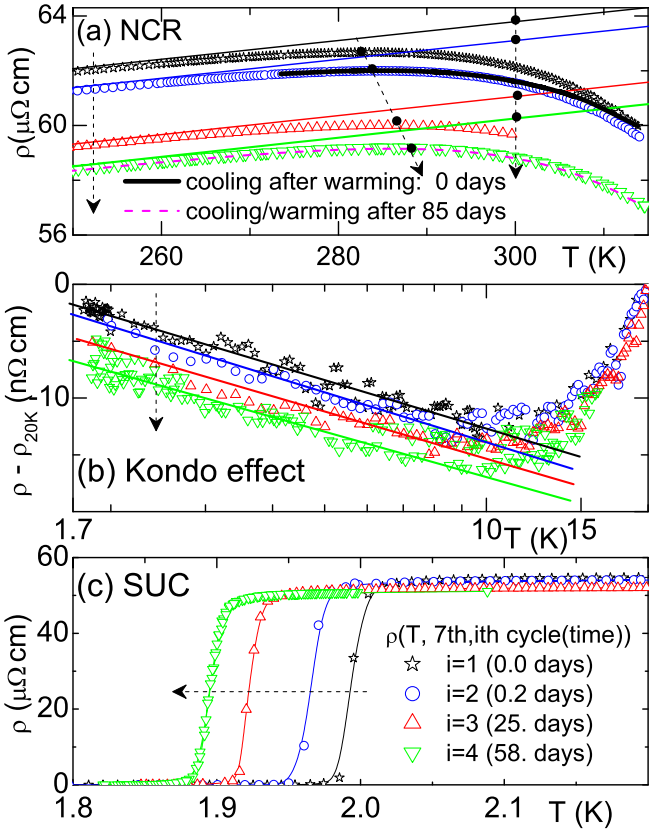

FIG. 4. Manifestation of the influence of aging on the three main feature of the phase diagrams. The ith cycle represents the order and time (in days) of the cooling-warming measurement carried out after the 7th irradiation session. (a) The influence of aging on the position and height of the peak maximum of NCR. The thick black line is the cooling curve directly after the first, $i = 1$, warming-up measurement while the red dashed line is the cooling and warming curves of $i = 5$ cycle after 85 days. The solid thin straight lines are linear fits within the range $100 \leqslant T \leqslant 220$ K. The solid circles represent each of $\rho(T_{\rm NCR}, 0{\rm kOe}, 7{\rm th}, i{\rm th})$ and $\rho^{\rm ext}_{300\,\rm K}(0{\rm kOe}, 7{\rm th}, i{\rm th})$. (b) Thermal evolution of $\rho(T, 5\ {\rm kOe}, 7{\rm th}, i{\rm th}) - \rho(20\ {\rm K}, 0\ {\rm kOe}, 7{\rm th}, i{\rm th})$ in a semilog plot. For $T < 10$ K, this shows a *log-in-T* dependence which is not a quantum localization effect since our film does not manifest a 2-dimensional character. (c) The degradation of $T_{\rm c}$ with aging. The arrows highlight the tendency of aging influence while the solid lines in panels (b) and (c) are guides to the eye. Just as for $T_{\rm NCR}$ of panel (a), there is no appreciable change in $T_{\rm K}^{\rm min}$ and $T_{\rm c}$ for $t > 85$ days.

or hole pairs (trapped near an oxygen ion which is adjacent to Al^{3+} vacancy) [16]. After reaching a steady state, such a disassociation-association process is reversible, leading to a reproducible NCR peak at $T_{\rm NCR}$. It is worth mentioning that studies on γ-irradiated Al_2O_3 identified a thermally assisted dissociation of hole pairs into single hole at 384 K and an annihilation of holes at 533 K [16].

C. The Kondo behavior

On lowering the temperature much below $T_{\rm K}^{\rm min}$, we observed a *log-in-T* feature [Fig. 4(b)] as well as a negative magnetoresistivity [Figs. 3(e) and 3(f)] that scales with $\sqrt{H/T}$ rather than the expected $(H/T)^2$. Same $\sqrt{H/T}$ scaling can be observed in magnetoresistivity of granular films with $\rho_{300\,\rm K} < 100\,\mu\Omega\,{\rm cm}$ (i.e., within a range similar to ours) [4]. As that we did not observe a $T^{-3/2}$ dependence, that the *log-in-T* contribution and $T_K^{\rm min}$ occur at a relatively high-T range, and that our films are considered to be $3d$, we do not associate this scaling to a localization stemming from $2d$ quantum corrections. More compelling evidence of a Kondo-like behavior is the direct observation, by Bachar *et al.* [3,4], of free spins in oxygen-incorporated granular Al films. Similar to the NCR case, the Kondo behavior become more accentuated on subsequent nth irradiation [but degraded by aging as in Fig. 4(b)].

We associate this Kondo contribution to scattering off irradiation-induced paramagnetic, color-center-type, defects located at the interface between Al and Al_2O_3 grains. It is recalled that magnetic defects located at the Al-Al_2O_3 interface had been suggested by various workers who studied the $1/f$ flux noise in Al-based SQUID [19]. Moreover, such magnetic centers were observed in irradiated Al_2O_3 by electron spin resonance studies and were attributed to either unpaired electrons which are trapped at an anion vacancy or to a hole trapped near an oxygen ion which is adjacent to Al^{3+} vacancy [16]. On assuming that implantation has introduced complexes [20] (e.g., Al_2O_3), which are capable of stabilizing these centers (see Fig. 1), one is able to explain the following: (i) Kondo behavior is not observed in pure Al films, not even when these are irradiated with nonchemically active projectiles. (ii) Kondo behavior is absent at the lower left-hand side of Fig. 5. Here the metallic and screening character are sufficiently strong to oppose the formation of paramagnetic centers. Finally, (iii) the surge, operation, and manifestation of a Kondo process is similar in both the granular and irradiated films: Indeed, a plot of the obtained minimum point of resistivity, $T_{\rm K}^{\rm min}$, versus $\rho^{\rm ext}_{300\,\rm K}$ in Fig. 5 evolves smoothly and extrapolates directly into a $T_{\rm K}^{\rm min} - \rho_{300\,\rm K}$ curve taken from Refs. [3,4].

D. The enhancement of $T_{\rm c}$

Figure 3(c) illustrates the accentuation of $T_{\rm c}$ enhancement with the subsequent nth irradiation: Note that the superconducting transitions width ($\Delta T_c^{10-90\%} < 80$ mK) is sharp and that superconductivity is quenched on an application of $H > H_{c2}(T, n{\rm th}) \approx 5$ kOe. Figures 4(c), on the other hand, demonstrates $T_{\rm c}$ decrease with aging.

Figure 5 summaries the $T_{\rm c}$ enhancement as obtained from this work [see Fig. 3(c)] as well as those reported on granular [1–4] and irradiated films [6]. It is remarkable that all data, new and old, follow the same phase boundaries across the whole available region: This finding is far from being trivial.

Evidently, $T_{\rm c}$ is enhanced monotonically at lower oxygen incorporation, passes through a maximum, and afterwards decreases monotonically. Numerous theoretical models were suggested for the explanation of T_c enhancement [see, e.g., Refs. [1,2,21–24]. One of these relates T_c enhancement to quantum-size effects in shell structures [24] but various studies, including this work, indicate that grain-size character (spatial confinement) is not a decisive factor in T_c

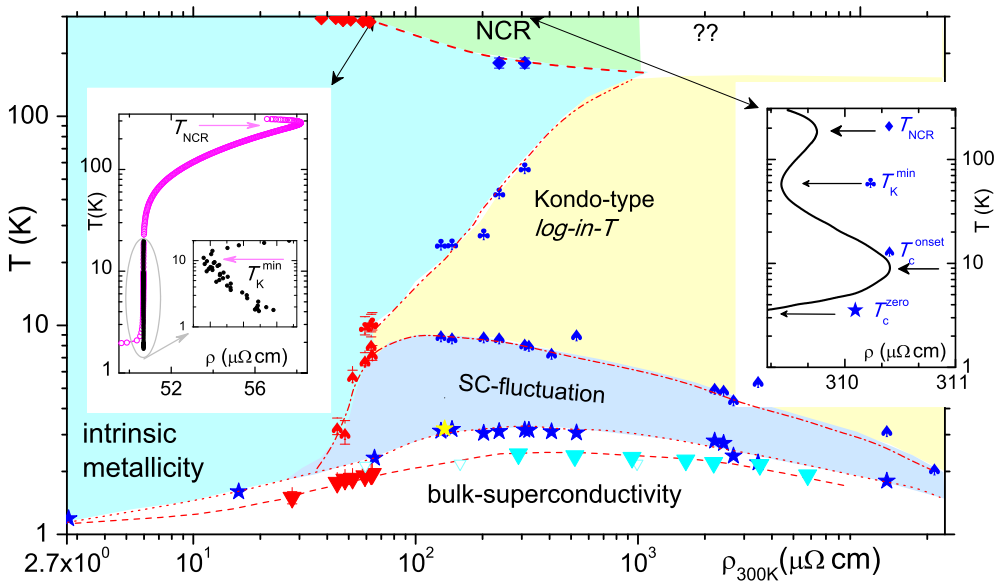

FIG. 5. Normal-state and superconducting phase diagram of different Al thin films shown as a log-log plot of T vs ρ_{300K}. ▼, ♠, ♣, ♦: T_c^{zero}, $T_c^{onset}(= T_K^{max})$, T_K^{min}, T_{NCR}, resp., as obtained by this work. ★, ♠, ♣, ♦: T_c^{zero}, $T_c^{onset}(= T_K^{max})$, T_K^{min}, T_{NCR}, resp., of granular films deposited at 77 K (Refs. [3,4]). The location of each thermal event is explicitly shown at the right-side inset. ▽,▼: T_c of granular films deposited at room-temperature (Refs. [5] and [17], resp.). ★: T_c after O implantation at liquid helium (Ref. [6]). Left-hand-side inset: A semilog plot of our irradiated film's $\rho(T,6\text{th},0\text{ kOe})$ and $\rho(T,6\text{th},5\text{ kOe})$ (open and close circles, resp.). Right-hand-side inset: A semilog plot of $\rho(T)$ curve of a granular sample having $\rho_{300\,K} = 310\ \mu\Omega$ cm (taken from Refs. [3,4]). The main graph is extrapolated down to 2.75 $\mu\Omega$ cm of bulk Al [18]. The lines are guides to the eye.

enhancement. Magnetic-based mechanisms can also be ruled out since T_c enhancement in Fig. 5 occurs much earlier than the region wherein possible magnetic fluctuation, if any, is expected. The BCS mechanism [22], on the other hand, cannot be excluded since it describes successfully the superconductivity of elemental Al and, by extension, the lower limit of this phase diagram (left-hand side of T_c dome of Fig. 5). Then, using a weak-limit BCS approximation, one expects to identify the essential ingredient behind T_c enhancement. A variation in $\partial T_c(\partial x)$ can be expressed in terms of a sum of a variation in Debye temperature θ_D, in the pairing potential V arising from electron-phonon coupling λ, and in the density of states N_F at Fermi energy:

$$\frac{\partial \ln T_c}{\partial x} = \frac{\partial \ln \theta_D}{\partial x} + \frac{1}{V N_F}\left(\frac{\partial \ln V}{\partial x} + \frac{\partial \ln N_F}{\partial x}\right). \quad (2)$$

The Hall effect [10] and specific heat [25] measurements on granular films indicated that N_F decreases with x. Our Hall curves in Fig. 3(d) do confirm this trend: While R_H of as-prepared film is the same as -3.4×10^{-13} Ω cm/G of pure Al, that of irradiated one is more negative and exhibits an upturn above T_{NCR}. θ_D also decreases with x [25]. Then, T_c enhancement must be related to an increase in V which, in turn, is related to λ [26]. Indeed, Fig. 3(b) confirms this increase in λ by demonstrating an increase in the metallic slope [27] $(\partial\rho/\partial T)_{100\text{-}220\,K}$ with x. In fact, it is almost *three times* higher than the 12 nΩ cmK^{-1} reported for bulk Al [18].

We associate such an increase in λ, V, and T_c enhancement [22,28] to a softening of the lattice, which is facilitated by the presence of vacancies that are created and stabilized during the *oxidation-like* process. Thus aging of T_c is driven by partial removal of these softening-inducing defects (by recombination, sinking, etc. [13]). The presence of such an aging process explains the manifestation of two $T_c(x)$ branches in Fig. 5: One branch is associated with $T_c^{>T_{NCR}}$ of films deposited or irradiated above T_{NCR} [5,17], while the other with $T_c^{<T_{NCR}}(x)$ of films deposited or irradiated below T_{NCR} [3,4,6]. Evidently aging effects lead to $T_c^{>T_{NCR}}(x) < T_c^{<T_{NCR}}(x)$; this is also evident in that the evolution of our $T_c^{zero}(x)$ (prepared and irradiated at 300 K) is in excellent agreement with that of $T_c^{>T_{NCR}}(x)$ [5,17]. Remarkably, each of $T_c^{>T_{NCR}}(x)$ and $T_c^{<T_{NCR}}(x)$ follows a dome-like evolution [7] when plotted on a log-log scale; the maximum is attained at 2.3 K (Ref. [17]) for the former while at 3.2 K (Refs. [3,4]) for the latter.

IV. FURTHER DISCUSSION AND SUMMARY

Impurities in an O-irradiated Al film consist mainly of implantation-induced chemical complexes [20]. Then, most of impurity-stabilized defects should be located at the border between, e.g., Al_2O_3 and metallic grains. These impurity-stabilized defects are assumed to consist of paramagnetic centers, trapped electrons, trapped holes or hole pairs, or vacancies (see Fig. 1). A reduction of these defects by any recombination or annihilation process would lead to (i) a reduction of scattering centres (aging of $\rho_{300\,K}$), (ii) a reduction of the thermally assisted liberation or annihilation of trapped charges above T_{NCR} (aging of NCR), (iii) a reduction of the paramagnetic centers (lowering of T_K), and (iv) a reduction in lattice softening (degradation of T_c).

It is notable that the surge of Kondo behavior occurs just below the dome maximum of Fig. 5 [3,4,7] and that the

monotonic evolution of Kondo effect is accompanied by a slowing down, leveling out, and eventual decay of $T_c(x)$. Accordingly, the domelike evolution of $T_c(x)$ is attributed to a compromise between an enhancement trend (due to lattice softening) and a suppression trend (due to Abrikosov-Gorkov pair-breaking process). As $T \rightarrow T_c^+$ ($T < T_K^{min}$), a competition between spin-flip scattering and Cooper pairing leads to a downward deviation away from the *log-in-T* behavior and as such to an eventual resistivity maximum at T_K^{max} (see right-hand side inset of Fig. 5). When the Kondo effect is weak, it is difficult to distinguish between T_K^{max} and T_c or T_c^{onset}. In this work we followed the evolution of $T_c^{onset}(\rho_{300\,K},nth)$ within the region starting just before the strong surge of Kondo behavior. Figure 5 indicates that the extrapolation of this $T_c^{onset}(\rho_{300\,K})$ agrees satisfactorily with the evolution of $T_K^{max}(\rho_{300\,K})$ reported for granular films [3,4]. We identify this range, $T_c^{zero} \leqslant T \leqslant T_K^{max}$, of Fig. 5 as being a superconducting fluctuation region.

In summary, an incorporation of a chemically active oxygen in Al thin films leads to a negative curvature resistivity, Kondo behavior, and enhancement of T_c. The obtained $T - x$ phase diagram is shown to be similar in both the granular and irradiated films. The driving mechanisms behind each of the involved processes as well as the aging effects are discussed.

ACKNOWLEDGMENTS

We gratefully acknowledge the technical assistance of K. S. F. M. Araújo and the use of the facilities at LABNANO-CBPF. Partial financial support from the Brazilian agencies CNPq and FAPERJ is also gratefully acknowledged.

[1] B. Abeles, P. Sheng, M. Coutts, and Y. Arie, Adv. Phys. **24**, 407 (1975).
[2] G. Deutscher, in *Superconductivity*, edited by K. Bennemann and J. Ketterson (Springer, Berlin, 2008), p. 259.
[3] N. Bachar, S. Lerer, A. Levy, S. Hacohen-Gourgy, B. Almog, H. Saadaoui, Z. Salman, E. Morenzoni, and G. Deutscher, Phys. Rev. B **91**, 041123 (2015); N. Bachar, S. Lerer, S. Hacohen-Gourgy, B. Almog, and G. Deutscher, *ibid.* **87**, 214512 (2013); U. S. Pracht, N. Bachar, L. Benfatto, G. Deutscher, E. Farber, M. Dressel, and M. Scheffler, *ibid.* **93**, 100503 (2016).
[4] N. Bachar, Spin-flip scattering in superconducting granular aluminum films, Ph.D. thesis, Tel-Aviv University, Tel-Aviv, Israel, 2014 (unpublished).
[5] B. Abeles, R. W. Cohen, and W. R. Stowell, Phys. Rev. Lett. **18**, 902 (1967).
[6] A. Lamoise, J. Chaumont, F. Meunier, and H. Bernas, J. Phys. Lett. **36**, 271 (1975); A. Lamoise, J. Chaumont, F. Lalu, F. Meunier, and H. Bernas, *ibid.* **37**, 287 (1976); A. Lamoise, J. Chaumont, F. Meunier, and H. Bernas, *ibid.* **36**, 305 (1975); F. Meunier, P. Pfeuty, A. Lamoise, J. Chaumont, H. Bernas, and C. Cohen, *ibid.* **38**, 435 (1977).
[7] G. Deutscher, M. Gershenson, E. Grunbaum, and Y. Imry, J. Vac. Sci. Technol. **10**, 697 (1973); G. Deutscher, H. Fenichel, M. Gershenson, E. Grünbaum, and Z. Ovadyahu, J. Low Temp. Phys. **10**, 231 (1973).
[8] K. Isebeck, R. Muller, W. Schilling, and H. Wenzl, Phys. Status Solidi **18**, 427 (1966); A. Sosin and L. H. Rachal, Phys. Rev. **130**, 2238 (1963); W. DeSorbo and D. Turnbull, *ibid.* **115**, 560 (1959); A. Khellaf, A. Seeger, and R. M. Emrick, Mater. Trans. **43**, 186 (2002).
[9] S. L. A. Mello, C. F. S. Codeco, B. F. Magnani, and M. M. Sant'Anna, Rev. Sci. Instrum. **87**, 063305 (2016).
[10] B. Bandyopadhyay, P. Lindenfeld, W. L. McLean, and H. K. Sin, Phys. Rev. B **26**, 3476 (1982).
[11] J. F. Ziegler, M. Ziegler, and J. Biersack, Nucl. Instrum. Methods B **268**, 1818 (2010).
[12] J. E. Boggio and R. C. Plumb, J. Chem. Phys. **44**, 1081 (1966).
[13] A. Atkinson, Rev. Mod. Phys. **57**, 437 (1985).
[14] A. Dorey and J. Knight, Thin Solid Films **4**, 445 (1969); M. E. Day, M. Delfino, J. A. Fair, and W. Tsai, *ibid.* **254**, 285 (1995).
[15] N. Cabrera and N. F. Mott, Rep. Prog. Phys. **12**, 163 (1949).
[16] F. T. Gamble, R. H. Bartram, C. G. Young, O. R. Gilliam, and P. W. Levy, Phys. Rev. **134**, A589 (1964); K. Lee, G. Holmberg, and J. Crawford, Solid State Commun. **20**, 183 (1976).
[17] T. Chui, P. Lindenfeld, W. L. McLean, and K. Mui, Phys. Rev. Lett. **47**, 1617 (1981); Phys. Rev. B **24**, 6728 (1981); K. C. Mui, P. Lindenfeld, and W. L. McLean, *ibid.* **30**, 2951 (1984).
[18] P. D. Desai, H. M. James, and C. Y. Ho, J. Phys. Chem. Ref. Data Rep. **13**, 1131 (1984).
[19] D. Lee, J. L. DuBois, and V. Lordi, Phys. Rev. Lett. **112**, 017001 (2014); S. M. Anton, J. S. Birenbaum, S. R. O'Kelley, V. Bolkhovsky, D. A. Braje, G. Fitch, M. Neeley, G. C. Hilton, H.-M. Cho, K. D. Irwin, F. C. Wellstood, W. D. Oliver, A. Shnirman, and J. Clarke, *ibid.* **110**, 147002 (2013); H. Bluhm, J. A. Bert, N. C. Koshnick, M. E. Huber, and K. A. Moler, *ibid.* **103**, 026805 (2009); S. Sendelbach, D. Hover, A. Kittel, M. Mück, J. M. Martinis, and R. McDermott, *ibid.* **100**, 227006 (2008).
[20] G. Linker and O. Meyer, Solid State Commun. **20**, 695 (1976); G. Linker, in *Ion Implantation into Metals*, edited by V. A. G. Procter (Pergamon, New York, 1982), pp. 284–292.
[21] I. S. Beloborodov, A. V. Lopatin, V. M. Vinokur, and K. B. Efetov, Rev. Mod. Phys. **79**, 469 (2007).
[22] J. W. Garland, K. H. Bennemann, and F. M. Mueller, Phys. Rev. Lett. **21**, 1315 (1968); J. Klein and A. Leger, Phys. Lett. A **28**, 134 (1968); A. Leger and J. Klein, *ibid.* **28**, 751 (1969).
[23] D. Allender, J. Bray, and J. Bardeen, Phys. Rev. B **7**, 1020 (1973).
[24] V. Z. Kresin and Y. N. Ovchinnikov, Phys. Usp. **51**, 427 (2008); S. Bose, A. M. García-García, M. M. Ugeda, J. D. Urbina, C. H. Michaelis, I. Brihuega, and K. Kern, Nat. Mater. **9**, 550 (2010); J. Mayoh and A. M. García-García, Phys. Rev. B **90**, 134513 (2014).
[25] R. L. Greene, C. N. King, R. B. Zubeck, and J. J. Hauser, Phys. Rev. B **6**, 3297 (1972).
[26] W. L. McMillan, Phys. Rev. **167**, 331 (1968).
[27] P. B. Allen, T. P. Beaulac, F. S. Khan, W. H. Butler, F. J. Pinski, and J. C. Swihart, Phys. Rev. B **34**, 4331 (1986).
[28] B. T. Matthias, G. R. Stewart, A. L. Giorgi, J. L. Smith, Z. Fisk, and H. Barz, Science **208**, 401 (1980).